Received 19 November 2007
Revised 28 July 2008
Accepted 12 August 2008

# Numerical prediction of periodically developed fluid flow and heat transfer characteristics in the sinusoid wavy fin-and-tube heat exchanger

Y.P. Cheng, T.S. Lee and H.T. Low
*Laboratory of Fluid Mechanics, Department of Mechanical Engineering, National University of Singapore, Singapore*

## Abstract

**Purpose** – In this paper three-dimensional numerical simulations were conducted for the periodically developed laminar flow in the sinusoid wavy fin-and-tube heat exchanger.

**Design/methodology/approach** – A novel CLEARER algorithm is adopted to guarantee the fully coupling between the pressure and velocity, and it can not only speed up the convergence rate, but also overcome the severe grid non-orthogonality in the wavy fin-and-tube heat exchanger. The influence of wave amplitude, fin pitch, tube diameter and wave density on fluid flow and heat transfer characteristics is analyzed under different Reynolds numbers.

**Findings** – The numerical results show that with the increase of wave amplitude, tube diameter or wave density, both the friction factor and Nusselt number will increase, and the increase rate of friction factor is higher than that of Nusselt number. It is interesting to note that, at low Reynolds numbers the Nusselt number increases with the decrease of fin pitch, while at high Reynolds numbers, the Nusselt number increases with the increase of fin pitch.

**Originality/value** – The numerical results presented in this paper may provide some useful guidance in the design of the wavy fin-and-tube heat exchanger with large number of rows of tubes.

**Keywords** Programming and algorithm theory, Numerical analysis, Simulation, Heat exchangers, Flow

**Paper type** Research paper

## 1. Introduction

Plate fin-and-tube heat exchangers are widely employed in various engineering applications, such as air conditioning, refrigeration, compressor intercoolers. In the overall thermal resistance, the airside thermal resistance is usually dominant. As a result, in order to enhance overall heat transfer rate and also to reduce the size and weight of heat exchangers, different types of enhanced heat transfer fins are often adopted, such as wavy fin, louvered fin and slit fin. Because wavy fin is easy to manufacture due to its simple geometric shape, it is popularly used in heat transfer enhancement.

So far many researchers have studied wavy fin-and-tube heat exchangers by experiments. The early study was conducted by Beecher and Fagan (1987), who tested 21 samples of wavy fin-and-tube heat exchangers. However, in their experiment the fins were electrically heated to keep it at constant temperature, and the thermal resistance between tubes and fins was zero, hence their correlations cannot be widely adopted in practical design, later Webb (1990) used a multiple regression technique to correlate their experimental correlations. Wang *et al.* (1997, 1999b, 2002) made comprehensive studies on the performance of fluid flow and heat transfer in wavy fin-and-tube heat exchangers, and developed the accurate empirical correlations.

International Journal of Numerical Methods for Heat & Fluid Flow
Vol. 19 No. 6, 2009
pp. 728-744

0961-5539
DOI 10.1108/09615530910972986

Wongwises and Chokeman (2005) examined the effect of fin pitch and number of tube rows, and stated that the fin pitch has an insignificant influence on heat transfer performance. Kuvannarat *et al.* (2006) examined the effect of fin thickness in wavy fin-and-tube heat exchangers under dehumidifying conditions, and they proposed the empirical correlations. Furthermore, Pirompugd *et al.* (2006) studied the simultaneous heat and mass transfer characteristics under dehumidifying conditions, and they also provided the corresponding correlations. Recently, Dong *et al.* (2007) conducted the study on wavy fin-and-tube heat exchangers with flat tubes, and they examined the effects of fin pitch, fin height and fin length on the heat transfer and pressure drop performances; moreover, they also developed their correlations, which can predict 95 percent of the experimental data within ±10 percent.

All the studies stated above were conducted by experiments. It is quite expensive and time-consuming to investigate the performance of wavy fin-and-tube heat exchangers, because a wide range of geometric variation is needed to be produced. For example, a total of 61 samples containing approximately 570 data were used by Wang *et al.* (2002) to conduct a systematic study on the wavy fin-and-tube heat exchanger. However, numerical modeling, once validated by reliable experimental data, offers a cost-effective tool for such comprehensive studies. Hence great deals of efforts have been paid in this regard.

Jang and Chen (1997) numerically simulated the heat transfer and fluid flow in wavy fin-and-tube heat exchangers, and they analyzed the effects of different geometrical parameters, including tube row numbers, wavy angles and wavy heights under different Reynolds number. Min and Webb (2001) studied a wavy fin-and-tube heat exchanger with two rows of tubes using the FLUENT software, and they considered the heat conduction in the solid fin in their calculation. Their numerical results on heat transfer and pressure drop performance agree quite well with the test data taken by Kang and Webb (1998). Tao *et al.* (2007a) also simulated the laminar flow in the wavy fin-and-tube heat exchanger with body-fitted coordinates methods, the local Nusselt number and fin efficiency on the fin surfaces were analyzed in detail. Furthermore, Tao *et al.* (2007b) investigated the effects of Reynolds number, fin pitch, wavy angle and tube row number on the pressure drop and heat transfer performance.

Most of the previous studies on wavy fin-and-tube heat exchangers were focused on triangular wavy fin, while the smooth wavy fin was seldom addressed. In some cases the triangular wavy fin-and-tube heat exchanger cannot work well. For example, in the study conducted by Wang *et al.* (1999a) it was found that, compared with the plain fin-and-tube heat exchanger, the enhancement of heat transfer coefficient of the triangular wavy fin-and-tube heat exchanger with small wavy height is negligible at low inlet velocity, while the increase of corresponding pressure drop is quite significant. The study conducted by Kang *et al.* (1994) shows that the smooth wavy fin can own comparable performance with triangular fin. One purpose of this article is to study the performance of the smooth wavy fin-and-tube heat exchanger.

Furthermore, most of studies on wavy fin-and-tube heat exchangers are only confined to heat exchangers with only a few rows of tubes, however, in some industrial applications, such as compressor intercooler, the wavy fin-and-tube heat exchangers with a large number of rows of tubes are usually adopted to satisfy the practical requirement. The geometrical complexity brings great difficulty for both experimental study and numerical simulation. Another purpose of this article is to simulate the fluid flow and heat transfer of wavy fin-and-tube heat exchangers with a large number of rows of tubes.

In the following presentation, the physical model will first be presented, followed by the grid generation with body-fitted coordinate method; then the governing equations and numerical treatment will be introduced in detail; in the later numerical results the effects of wave amplitude, fin pitch, tube diameter and wave density on the fluid flow and heat transfer performance will be analyzed; finally, some conclusions will be drawn which are helpful in the design of wavy fin-and-tube heat exchanger.

## 2. Mathematical formulation

### *2.1 Physical model*

The schematic diagram of a typical sinusoidal wavy fin-and-tube heat exchanger is shown in Figure 1 and the cross section of a wavy fin-and-tube structure is presented in Figure 2. The parallel sinusoid fins are equally placed, and an array of tubes with staggered arrangement pass through the plates perpendicularly. The cooling air flows along the fin surfaces from the left, the hot water or refrigerant flows inside the tubes, and then the heat is transmitted to the cooling air through the tube and fin surface. Because the inlet velocity is usually quite low and the temperature variation in the fin-and-tube heat exchanger is insignificant, the flow is assumed to be incompressible laminar with constant physical property. The fins and tubes are usually made of copper or aluminum with high conductivity; hence the fins and tubes are regarded as constant temperature.

Due to the large number of rows of tubes and wavy fins, it is quite difficult to simulate the whole wavy fin-and-tube heat exchanger. Tao *et al.* (2007c) proposed a new method to divide the whole fin-and-tube heat exchanger into several stages along the flow direction, then simulated the heat exchanger stage by stage, but it is still quite challenging and time-consuming to numerically simulate the heat exchanger, especially that with large number of rows of tubes. It is notable that after a certain number of rows of tubes, the flow in the wavy fin-and-tube heat exchanger will become periodically developed, hence the numerical simulation can be simplified greatly. According to the geometrical periodicity, the cell between two adjacent wavy fins containing two tubes is investigated, as shown in the shadow area in Figure 2. In the numerical simulation this cell is regarded as the computation domain. Here $x$ is the streamwise coordinate, $y$ is the spanwise coordinate and $z$ is the fin pitch direction. The detailed simulation conditions of the wavy fin-and-tube heat exchanger are presented in Table I.

### *2.2 Grid generation*

For the fluid flow in regular geometry, such as rectangular, cylindrical and polar geometries, the corresponding orthogonal grid system can be applied directly. However, in this study the geometry of wavy fin-and-tube heat exchanger is quite

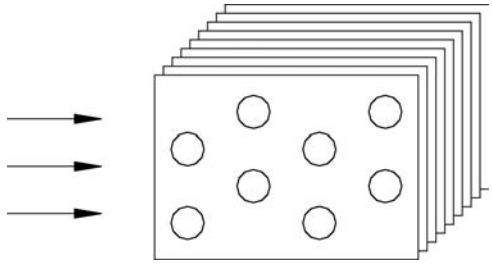

**Figure 1.**
Schematic diagram of a wavy fin-and-tube heat exchanger

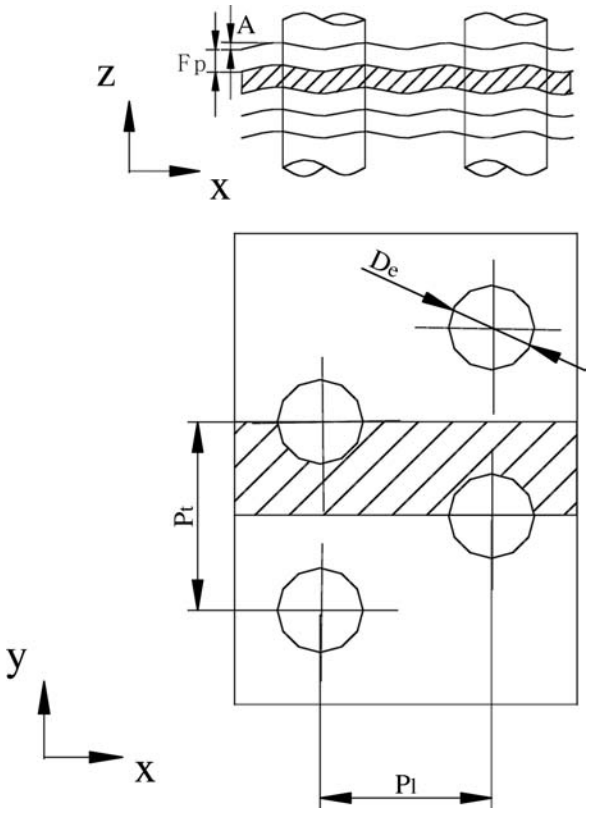


**Figure 2.**
Geometric parameters and computation domain

| | |
|---|---|
| Tube diameter $D_e$ | 8.8-13.6 mm |
| Longitudinal tube pitch $P_l$ | 22.4 mm |
| Transverse tube pitch $P_t$ | 25 mm |
| Fin pitch $F_p$ | 2.0-3.0 mm |
| Wave amplitude $A$ | 0-2.61 mm |
| Inlet velocity $u_{in}$ | 0.5-5 m/s |
| Inlet temperature $T_{in}$ | 293 K |
| Tube temperature $T_w$ | 303 K |

**Table I.**
Simulation conditions

complex, hence the body-fitted coordinate method is adopted, in which the non-uniform non-orthogonal physical space *x, y, z* can be mapped into the transformed uniform orthogonal computational space $\xi, \eta, \zeta$. The commonly used grid generation techniques are based on the Poisson equation proposed by Thomas and Middlecoeff (1980). The three-dimensional Poisson equations are expressed as follows:

$$\frac{\partial^2 \xi}{\partial x^2} + \frac{\partial^2 \xi}{\partial y^2} + \frac{\partial^2 \xi}{\partial z^2} = \phi(\xi, \eta, \zeta)|\nabla \xi|^2 \tag{1a}$$

$$\frac{\partial^2\eta}{\partial x^2}+\frac{\partial^2\eta}{\partial y^2}+\frac{\partial^2\eta}{\partial z^2}=\varphi(\xi,\eta,\zeta)|\nabla\eta|^2 \tag{1b}$$

$$\frac{\partial^2\zeta}{\partial x^2}+\frac{\partial^2\zeta}{\partial y^2}+\frac{\partial^2\zeta}{\partial z^2}=\omega(\xi,\eta,\zeta)|\nabla\zeta|^2 \tag{1c}$$

where $\phi, \psi, \omega$ are universal grid control parameters, and they can be used to control the grid density, their values can be calculated through the derivatives of $\xi, \eta, \zeta$. It is noted that for the irregular two-dimensional surface on the boundaries, the grid is generated with two-dimensional Poisson equations, similar to Equation (1).

The above equations in physical space can be transformed into the computational space, where the Cartesian coordinates are the dependent variables, as shown below:

$$\begin{aligned}&\alpha_{11}\left(x_{\xi\xi}+\phi x_{\xi}\right)+\alpha_{22}\left(x_{\eta\eta}+\varphi x_{\eta}\right)+\alpha_{33}\left(x_{\zeta\zeta}+\omega x_{\zeta}\right)\\&\quad+2\left(\alpha_{12}x_{\xi\eta}+\alpha_{13}x_{\xi\zeta}+\alpha_{23}x_{\eta\zeta}\right)=0\end{aligned} \tag{2a}$$

$$\begin{aligned}&\alpha_{11}\left(y_{\xi\xi}+\phi y_{\xi}\right)+\alpha_{22}\left(y_{\eta\eta}+\varphi y_{\eta}\right)+\alpha_{33}\left(y_{\zeta\zeta}+\omega y_{\zeta}\right)\\&\quad+2\left(\alpha_{12}y_{\xi\eta}+\alpha_{13}y_{\xi\zeta}+\alpha_{23}y_{\eta\zeta}\right)=0\end{aligned} \tag{2b}$$

$$\begin{aligned}&\alpha_{11}\left(z_{\xi\xi}+\phi z_{\xi}\right)+\alpha_{22}\left(z_{\eta\eta}+\varphi z_{\eta}\right)+\alpha_{33}\left(z_{\zeta\zeta}+\omega z_{\zeta}\right)\\&\quad+2\left(\alpha_{12}z_{\xi\eta}+\alpha_{13}z_{\xi\zeta}+\alpha_{23}z_{\eta\zeta}\right)=0\end{aligned} \tag{2c}$$

where $\alpha_{ij}=\sum_{m=1}^{3}\beta_{mi}\beta_{mj}$, and $\beta_{mi}$ is the cofactor of the (m, i) element in the following matrix:

$$M=\begin{bmatrix}x_{\xi} & x_{\eta} & x_{\zeta}\\ y_{\xi} & y_{\eta} & y_{\zeta}\\ z_{\xi} & z_{\eta} & z_{\zeta}\end{bmatrix}$$

Figure 3 shows the body-fitted grid system generated with above method. For convenience of display, only the coarse grid is provided. From which it can be seen that the grid quality is quite satisfactory, which lays solid ground for the later numerical simulation. It is noted that in order to simulate the flow fluid and heat transfer accurately, the grid near the fin surfaces and tubes is set finer.

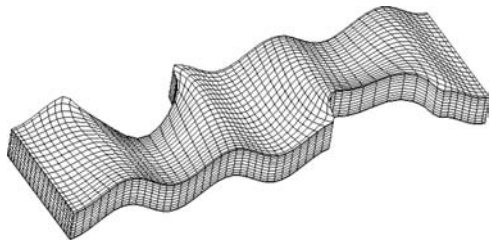

**Figure 3.**
Body-fitted grid system in numerical simulation

*2.3 Governing equations and boundary conditions*

The governing equations for three-dimensional steady incompressible laminar flow are as follows:

Continuity equation

$$\frac{\partial(\rho u)}{\partial x}+\frac{\partial(\rho v)}{\partial y}+\frac{\partial(\rho w)}{\partial z}=0 \tag{3}$$

Momentum equations

$$\frac{\partial(\rho uu)}{\partial x}+\frac{\partial(\rho vu)}{\partial y}+\frac{\partial(\rho wu)}{\partial z}=-\frac{\partial p}{\partial x}+\mu\left(\frac{\partial^2 u}{\partial x^2}+\frac{\partial^2 u}{\partial y^2}+\frac{\partial^2 u}{\partial z^2}\right) \tag{4a}$$

$$\frac{\partial(\rho uv)}{\partial x}+\frac{\partial(\rho vv)}{\partial y}+\frac{\partial(\rho wv)}{\partial z}=-\frac{\partial p}{\partial y}+\mu\left(\frac{\partial^2 v}{\partial x^2}+\frac{\partial^2 v}{\partial y^2}+\frac{\partial^2 v}{\partial z^2}\right) \tag{4b}$$

$$\frac{\partial(\rho uw)}{\partial x}+\frac{\partial(\rho vw)}{\partial y}+\frac{\partial(\rho ww)}{\partial z}=-\frac{\partial p}{\partial z}+\mu\left(\frac{\partial^2 w}{\partial x^2}+\frac{\partial^2 w}{\partial y^2}+\frac{\partial^2 w}{\partial z^2}\right) \tag{4c}$$

Energy equation

$$\frac{\partial(\rho uT)}{\partial x}+\frac{\partial(\rho vT)}{\partial y}+\frac{\partial(\rho wT)}{\partial z}=\frac{\lambda}{c_p}\left(\frac{\partial^2 T}{\partial x^2}+\frac{\partial^2 T}{\partial y^2}+\frac{\partial^2 T}{\partial z^2}\right) \tag{5}$$

The governing equations in the irregular physical domain can be transformed in the regular computational domain as follows:

Continuity equation

$$\frac{\partial(\rho U)}{\partial \xi}+\frac{\partial(\rho V)}{\partial \eta}+\frac{\partial(\rho W)}{\partial \zeta}=0 \tag{6}$$

Momentum equations

$$\begin{aligned}\frac{\partial(\rho Uu)}{\partial \xi}+\frac{\partial(\rho Vu)}{\partial \eta}+\frac{\partial(\rho Wu)}{\partial \zeta}&=-\left(\beta_{11}\frac{\partial p}{\partial \xi}+\beta_{12}\frac{\partial p}{\partial \eta}+\beta_{13}\frac{\partial p}{\partial \zeta}\right)\\&+\mu\left(\frac{\alpha_{11}}{J}\frac{\partial^2 u}{\partial \xi^2}+\frac{\alpha_{22}}{J}\frac{\partial^2 u}{\partial \eta^2}+\frac{\alpha_{33}}{J}\frac{\partial^2 u}{\partial \zeta^2}\right)+\mu\frac{\partial}{\partial \xi}\left(\frac{\alpha_{12}}{J}\frac{\partial u}{\partial \eta}+\frac{\alpha_{13}}{J}\frac{\partial u}{\partial \zeta}\right)\\&+\mu\frac{\partial}{\partial \eta}\left(\frac{\alpha_{12}}{J}\frac{\partial u}{\partial \xi}+\frac{\alpha_{23}}{J}\frac{\partial u}{\partial \zeta}\right)+\mu\frac{\partial}{\partial \zeta}\left(\frac{\alpha_{13}}{J}\frac{\partial u}{\partial \xi}+\frac{\alpha_{23}}{J}\frac{\partial u}{\partial \eta}\right)\end{aligned} \tag{7a}$$

$$\begin{aligned}\frac{\partial(\rho Uv)}{\partial \xi}+\frac{\partial(\rho Vv)}{\partial \eta}+\frac{\partial(\rho Wv)}{\partial \zeta}&=-\left(\beta_{21}\frac{\partial p}{\partial \xi}+\beta_{22}\frac{\partial p}{\partial \eta}+\beta_{23}\frac{\partial p}{\partial \zeta}\right)\\&+\mu\left(\frac{\alpha_{11}}{J}\frac{\partial^2 v}{\partial \xi^2}+\frac{\alpha_{22}}{J}\frac{\partial^2 v}{\partial \eta^2}+\frac{\alpha_{33}}{J}\frac{\partial^2 v}{\partial \zeta^2}\right)+\mu\frac{\partial}{\partial \xi}\left(\frac{\alpha_{12}}{J}\frac{\partial v}{\partial \eta}+\frac{\alpha_{13}}{J}\frac{\partial v}{\partial \zeta}\right)\\&+\mu\frac{\partial}{\partial \eta}\left(\frac{\alpha_{12}}{J}\frac{\partial v}{\partial \xi}+\frac{\alpha_{23}}{J}\frac{\partial v}{\partial \zeta}\right)+\mu\frac{\partial}{\partial \zeta}\left(\frac{\alpha_{13}}{J}\frac{\partial v}{\partial \xi}+\frac{\alpha_{23}}{J}\frac{\partial v}{\partial \eta}\right)\end{aligned} \tag{7b}$$

$$\begin{aligned}\frac{\partial(\rho Uw)}{\partial\xi}+\frac{\partial(\rho Vw)}{\partial\eta}+\frac{\partial(\rho Ww)}{\partial\zeta}&=-\left(\beta_{31}\frac{\partial p}{\partial\xi}+\beta_{32}\frac{\partial p}{\partial\eta}+\beta_{33}\frac{\partial p}{\partial\zeta}\right)\\&+\mu\left(\frac{\alpha_{11}}{J}\frac{\partial^2 w}{\partial\xi^2}+\frac{\alpha_{22}}{J}\frac{\partial^2 w}{\partial\eta^2}+\frac{\alpha_{33}}{J}\frac{\partial^2 w}{\partial\zeta^2}\right)+\mu\frac{\partial}{\partial\xi}\left(\frac{\alpha_{12}}{J}\frac{\partial w}{\partial\eta}+\frac{\alpha_{13}}{J}\frac{\partial w}{\partial\zeta}\right)\\&+\mu\frac{\partial}{\partial\eta}\left(\frac{\alpha_{12}}{J}\frac{\partial w}{\partial\xi}+\frac{\alpha_{23}}{J}\frac{\partial w}{\partial\zeta}\right)+\mu\frac{\partial}{\partial\zeta}\left(\frac{\alpha_{13}}{J}\frac{\partial w}{\partial\xi}+\frac{\alpha_{23}}{J}\frac{\partial w}{\partial\eta}\right)\end{aligned}\tag{7c}$$

Energy equation

$$\begin{aligned}&\frac{\partial(\rho UT)}{\partial\xi}+\frac{\partial(\rho VT)}{\partial\eta}+\frac{\partial(\rho WT)}{\partial\zeta}\\&=\frac{\lambda}{c_p}\left(\frac{\alpha_{11}}{J}\frac{\partial^2 T}{\partial\xi^2}+\frac{\alpha_{22}}{J}\frac{\partial^2 T}{\partial\eta^2}+\frac{\alpha_{33}}{J}\frac{\partial^2 T}{\partial\zeta^2}\right)+\frac{\lambda}{c_p}\frac{\partial}{\partial\xi}\left(\frac{\alpha_{12}}{J}\frac{\partial T}{\partial\eta}+\frac{\alpha_{13}}{J}\frac{\partial T}{\partial\zeta}\right)\\&+\frac{\lambda}{c_p}\frac{\partial}{\partial\eta}\left(\frac{\alpha_{12}}{J}\frac{\partial T}{\partial\xi}+\frac{\alpha_{23}}{J}\frac{\partial T}{\partial\zeta}\right)+\frac{\lambda}{c_p}\frac{\partial}{\partial\zeta}\left(\frac{\alpha_{13}}{J}\frac{\partial T}{\partial\xi}+\frac{\alpha_{23}}{J}\frac{\partial T}{\partial\eta}\right)\end{aligned}\tag{8}$$

Here $U$, $V$, $W$ are the contravariant velocities, and are defined as below:

$$U=\beta_{11}u+\beta_{21}v+\beta_{31}w \tag{9a}$$

$$V=\beta_{12}u+\beta_{22}v+\beta_{32}w \tag{9b}$$

$$W=\beta_{13}u+\beta_{23}v+\beta_{33}w \tag{9c}$$

$$J=\begin{vmatrix}x_\xi & x_\eta & x_\zeta\\ y_\xi & y_\eta & y_\zeta\\ z_\xi & z_\eta & z_\zeta\end{vmatrix} \tag{10}$$

The values of $\alpha$ and $\beta$ are consistent with those in grid generation.

Due to the elliptic governing equations, all the boundary conditions are required for the computation domain, and they are listed as follows:

At the inlet and outlet: the periodic boundary condition.

At the top and bottom:

$$u=v=w=0, T=T_{\mathrm{w}} \tag{11}$$

At the front and back sides

tube surface:

$$u=v=w=0, T=T_{\mathrm{w}} \tag{12}$$

other part:

$$u = \frac{\partial v}{\partial y} = w = 0, \frac{\partial T}{\partial y} = 0 \tag{13}$$

*2.4 Numerical methods and parameter definition*

The transformed governing equations are discretized with finite volume method (Patankar, 1980; Tao, 2000, 2001) on the regular computation domain. Due to the complex geometry of the wavy fin-and-tube heat exchanger, the non-orthogonality of grid is quite severe somewhere, hence it is not easy to converge with current SIMPLE-family algorithms. Recently, Cheng *et al.* (2007) proposed a novel algorithm named CLEARER algorithm on non-orthogonal curvilinear coordinates. With the simplified pressure correction equation, this algorithm can overcome the severe non-orthogonality, furthermore it can also speed up the convergence rate, and hence it is adopted in this study. In order to increase the accuracy of the solution, the second-order scheme SGSD (2002) is adopted to discretize the convection term. The convergence criterion for the velocities is that maximum mass residual of the cells divided by the inlet mass flow is less than $1 \times 10^{-6}$, and criterion for temperature is that difference between heat transfer rates obtained from one iteration and successive 50 iterations is less than $1 \times 10^{-7}$.

Some parameters are defined as follows:

$$\mathrm{Re} = \frac{\rho u_{\mathrm{m}} D_{\mathrm{e}}}{\mu} \tag{14}$$

$$Nu = \frac{hD_{\mathrm{e}}}{\lambda} \tag{15}$$

$$h = \frac{Q}{A_{\mathrm{t}} \Delta T} \tag{16}$$

$$Q = \dot{m} c_p (T_{\mathrm{in}} - T_{\mathrm{out}}) \tag{17}$$

$$f = \frac{\Delta p}{1/2 \rho u_{\mathrm{m}}^2} \cdot \frac{D_e}{L} \tag{18}$$

$$\Delta T = \frac{T_{\max} - T_{\min}}{\log(T_{\max}/T_{\min})} \tag{19}$$

where $u_{\mathrm{m}}$ is the mean velocity of minimum transverse area, $D_{\mathrm{e}}$ is the tube diameter, and $T_{\mathrm{in}}$, $T_{\mathrm{out}}$ are the bulk temperature at the inlet and outlet, here $T_{\max} = \max(T_{\mathrm{w}} - T_{\mathrm{in}}, T_{\mathrm{w}} - T_{\mathrm{out}})$, $T_{\min} = \min(T_{\mathrm{w}} - T_{\mathrm{in}}, T_{\mathrm{w}} - T_{\mathrm{out}})$.

## 3. Results and discussions

*3.1 Validation of the code and mesh independent of the solution*

To validate the computational model and code developed, preliminary computations were conducted for the fluid flow in the triangular wavy fin-and-tube heat exchanger. For convenience of comparison the uniform velocity and temperature distribution at the entrance is assumed, which is consistent in the experimental study conducted by Wang *et al.* (2002). From Figures 4 and 5 it can be seen that the predicted Nusselt numbers in present study agree quite well with those in experimental study, while the

predicted friction factors deviate a little from the experimental values, but the average deviation is within 13 percent, which is acceptable for the complex fluid flow and heat transfer characteristics.

In order to adopt an appropriate grid system, a grid refinement was conducted to investigate the influence of the grid density on the computational results. Take the case

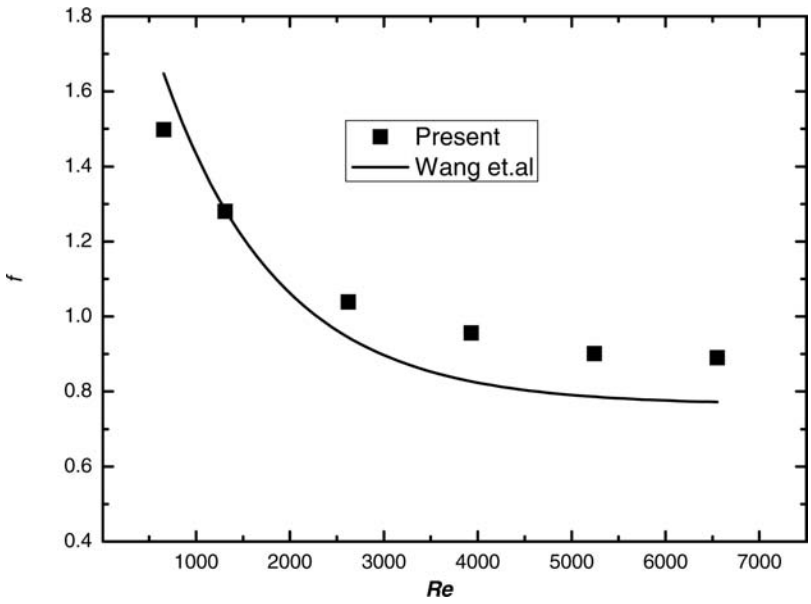


**Figure 4.**
Comparison between predicted and experimental friction factors

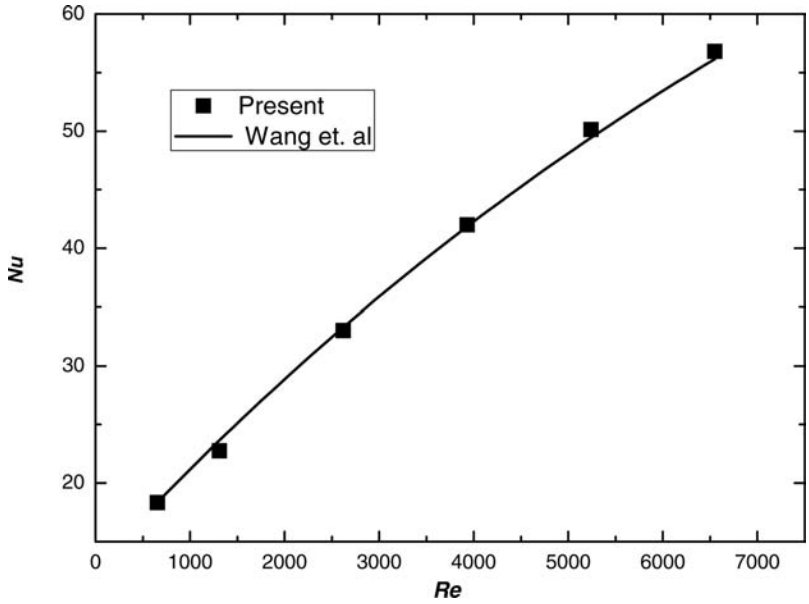


**Figure 5.**
Comparison between predicted and experimental Nusselt numbers

at $u_0 = 2\,\text{m/s}, F_P = 2.4\,\text{mm}, A = 1.76\,\text{mm}, D_e = 11.2\,\text{mm}$ as example, the friction factor on grid $114 \times 34 \times 22$ is 1.134, which is about 2.6 percent higher than 1.105 on the finer grid $114 \times 34 \times 42$; meanwhile, the Nusselt number on grid $114 \times 34 \times 22$ is 28.12, about 1.3 percent higher than 27.76 on the finer grid $114 \times 34 \times 42$. Therefore, in order to save the computational resource, the grid system $114 \times 34 \times 22$ is adopted in the following computations. The reference case is set with those parameters, $A = 1.76\,\text{mm}, F_P = 2.4\,\text{mm}, D_e = 11.2\,\text{mm}$ and wave number $n = 2$.

*3.2 Influence of wave amplitude*

In Figure 6 the friction factors of two wavy fin-and-tube heat exchangers with different wave amplitude are compared with those of the plain fin-and-tube heat exchanger under different Reynolds numbers. It is clear from this figure that with the increase of Reynolds number, all friction factors decrease mildly. Compared with the plain fin-and-tube heat exchanger, the increase of friction factors for two wavy fin-and-tube heat exchangers at low Reynolds numbers is not as significant as that at high Reynolds numbers. For example, at $\text{Re} = 655$, the friction factor of wavy fin-and-tube heat exchanger with $A = 1.76\,\text{mm}$ is only about 35 percent higher than that of plain fin-and-tube heat exchanger, while at $\text{Re} \geq 2,620$, the friction factor is about 80 percent higher. It is notable that the wave amplitude has great influence on the friction factor. When the wave amplitude is increased from 1.76 to 2.71mm, the friction factor will be increased by 45 percent.

In Figure 7 the heat transfer performance of two wavy fin-and-tube heat exchangers is compared with that of plain fin-and-tube heat exchanger under different Reynolds numbers. At low Reynolds number, the difference of Nusselt numbers among three fin-and-tube heat exchangers is not as large as that at high Reynolds numbers. In the

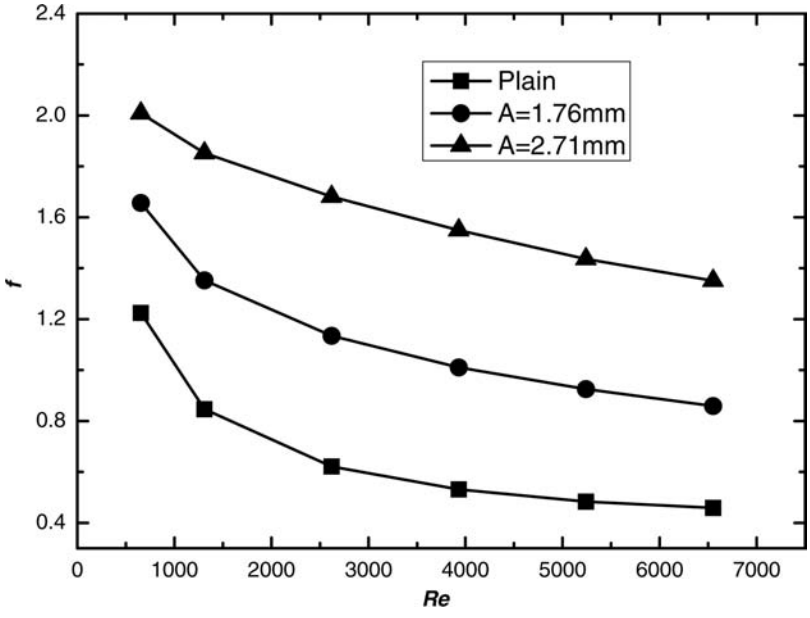


**Figure 6.**
Influence of wave amplitude on the friction factor under different Reynolds numbers

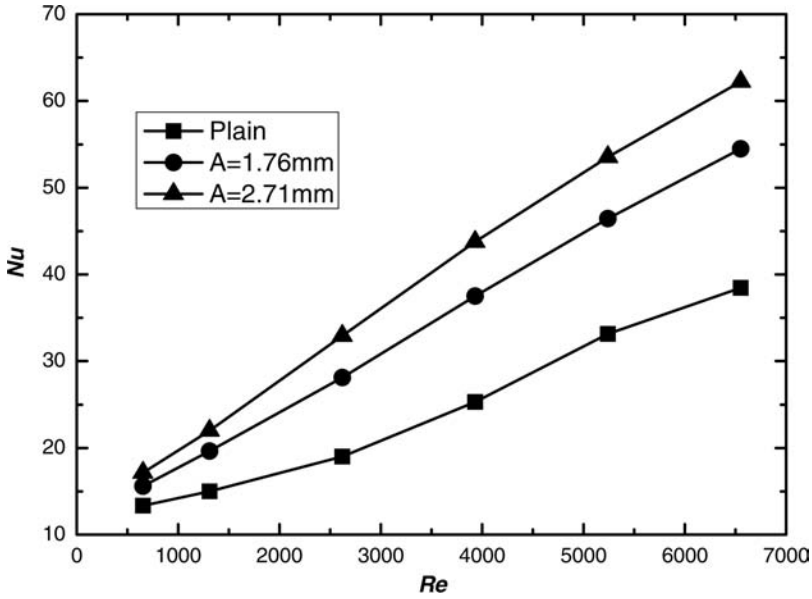


**Figure 7.**
Influence of wave amplitude on the Nusselt number under different Reynolds numbers

variation range of Reynolds number, the wavy fin-and-tube heat exchanger with $A = 1.76$ mm has 37 percent higher Nusselt number than plain fin-and-tube heat exchanger, while the wavy fin-and-tube heat exchanger with $A = 2.71$ mm has averaged 57 percent higher Nusselt number. Therefore, wavy fin is an effective method to enhance heat transfer, but it is often accompanied with higher pressure drop penalty.

*3.3 Influence of fin pitch*

Figure 8 shows the influence of fin pitch on friction factor under different Reynolds numbers for the wavy fin-and-tube heat exchanger with $A = 1.76$ mm. It is apparent that the larger the fin pitch is, the lower the friction factor. In the variation range of Reynolds number, the friction factor of the wavy fin-and-tube heat exchanger with $F_P = 2.4$ mm is averagely 10 percent lower than that with $F_P = 2.0$ mm, and the friction factor of the wavy fin-and-tube heat exchanger with $F_P = 3.0$ mm is averagely 20 percent lower.

In Figure 9 the Nusselt number of three wavy fin-and-tube heat exchangers with different fin pitch is compared under different Reynolds numbers. At low Reynolds numbers, the Nusselt number of the wavy fin-and-tube heat exchanger with smallest fin pitch is the highest, which is consistent with the traditional viewpoint. However, at high Reynolds numbers, the Nusselt number is the lowest in the wavy fin-and-tube heat exchanger with smallest fin pitch. When Reynolds number is greater than 3,931, the Nusselt number of wavy fin-and-tube heat exchanger with $F_P = 2.4$ mm is about 10 percent higher than that with $F_P = 2.0$ mm, while the Nusselt number of the wavy fin-and-tube heat exchanger with $F_P = 3.0$ mm is about 20 percent higher. Similar effects of fin pitch on the heat transfer performance can be observed when the wave amplitude, tube diameter and wave density are changed. Therefore, in the wavy fin-and-tube heat exchanger with periodically developed flow, the large fin pitch is preferred, not only due to its low pressure drop, but also due to its high heat transfer rate.

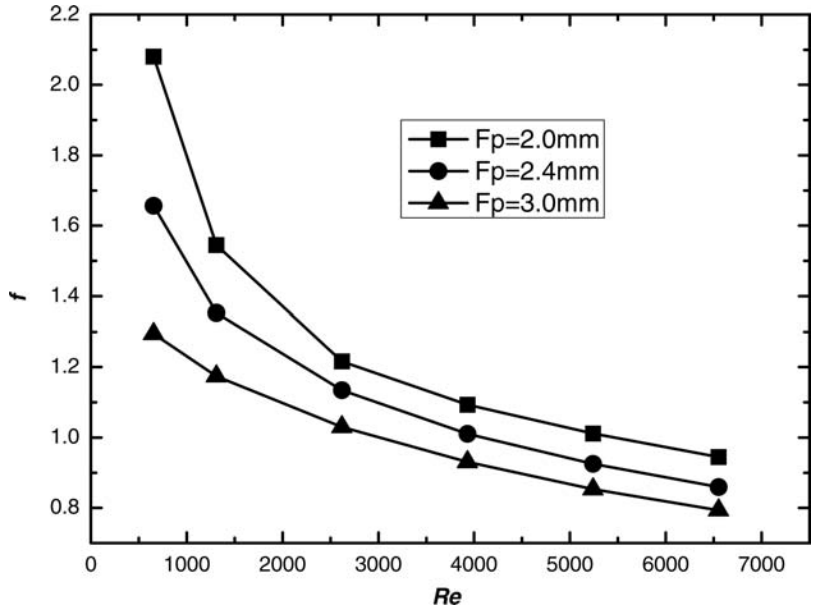


**Figure 8.**
Influence of fin pitch on the friction factor under different Reynolds numbers

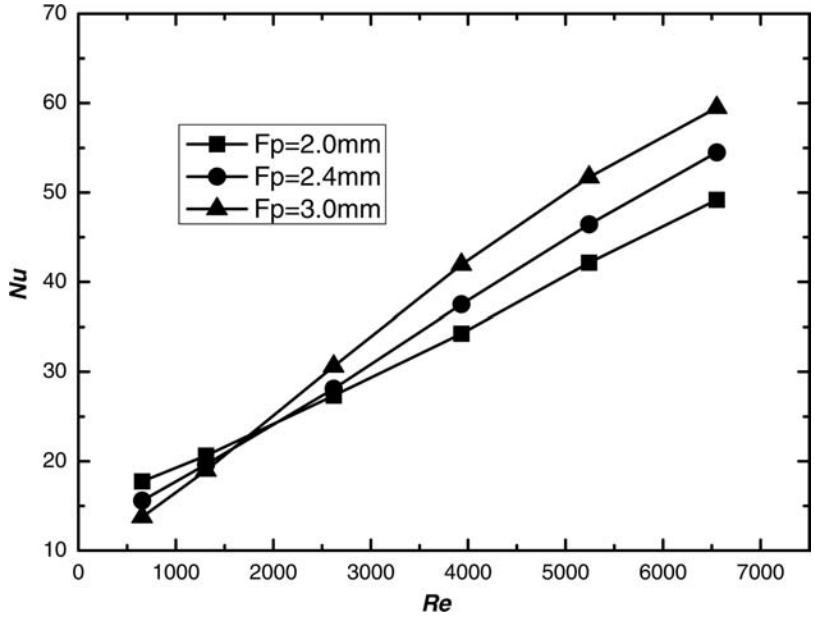


**Figure 9.**
Influence of fin pitch on the Nusselt number under different Reynolds numbers

*3.4 Influence of tube diameter*

In Figure 10 the influence of tube diameter of wavy fin-and-tube heat exchangers is shown under different Reynolds numbers. It can be seen that with the increase of tube diameter, the friction factor will increase, a result that is expected. Compared with the

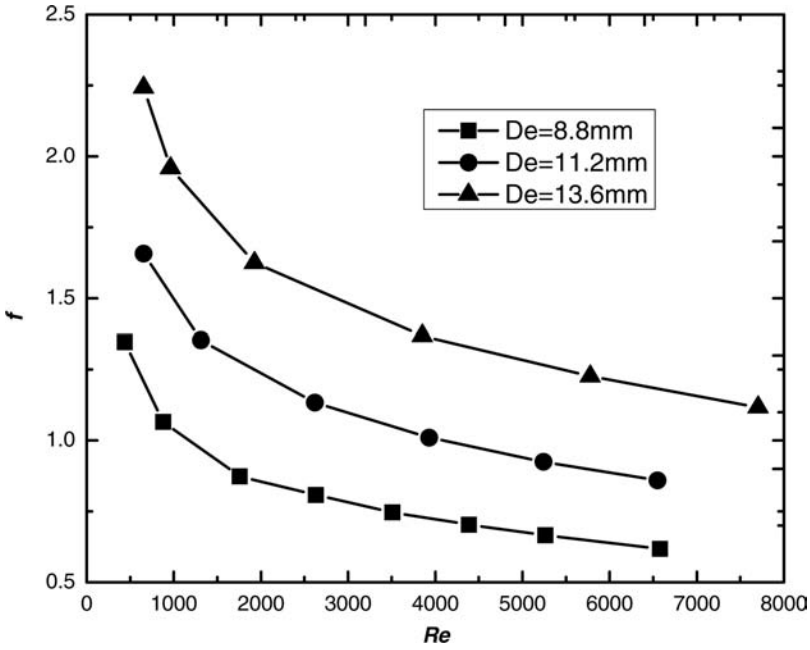


**Figure 10.**
Influence of tube diameter on the friction factor under different Reynolds numbers

wavy fin-and-tube heat exchanger, the increase ratio of friction factors of other two wavy fin-and-tube heat exchangers almost keeps constant in the variation range of Reynolds number. For example, the friction factor of the wavy fin-and-tube heat exchanger with $D_e = 11.2$ mm is about 33 percent higher than that with $D_e = 8.8$ mm, and the friction factor of the wavy fin-and-tube heat exchanger with $D_e = 13.6$ mm is about 83 percent higher.

The influence of tube diameter on Nusselt number under different Reynolds numbers is shown in Figure 11, from which it can be seen that, during the variation range of Reynolds number the Nusselt number of the wavy fin-and-tube heat exchanger with $D_e = 11.2$ mm is averagely 21 percent higher than that with $D_e = 8.8$ mm, and the Nusselt number of the wavy fin-and-tube heat exchanger with $D_e = 13.6$ mm is averagely 33 percent higher. It is notable that the increase of Nusselt number is much lower than that of friction factor.

*3.5 Influence of wave density*

From Figures 12 and 13 it is seen that the wavy density in streamwise direction owns great influence on both the friction factor and Nusselt number. The numerical results are compared with one, two, and four wave numbers in one period. In the range of Reynolds number, the friction factor of the wavy fin-and-tube heat exchanger with four waves is much higher than that of other two wavy fin-and-tube heat exchangers. For example, at Re = 6,551 the friction factor of the wavy fin-and-tube heat exchanger with four waves is as much as five times higher than that of the wavy fin-and-tube heat exchanger with only one wave. Because the waviness can lengthen the flow path greatly; the more the waves are, the longer the flow path, which results in the larger friction factor.

From Figure 13 it can be seen that the Nusselt number of the wavy fin-and-tube heat exchanger with four waves is also much higher than that of other two wavy fin-and-tube

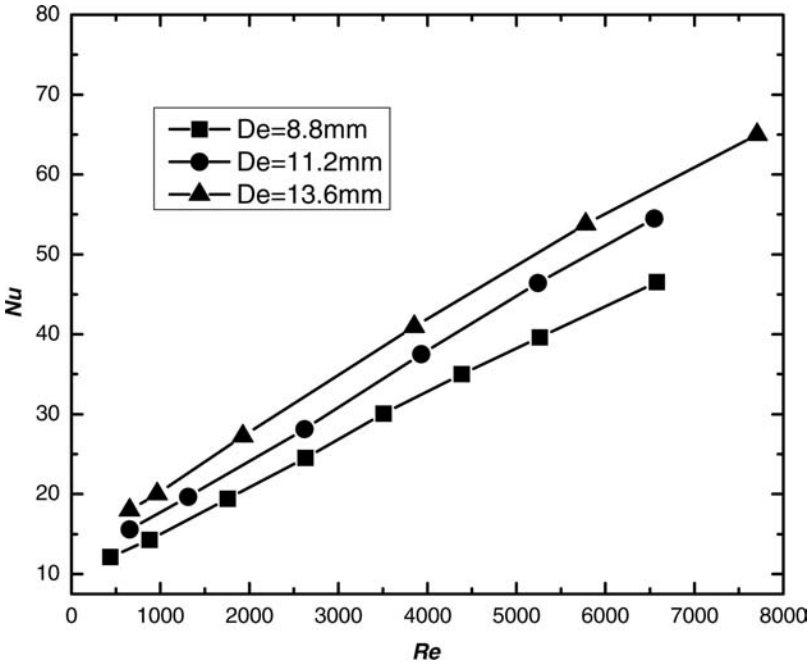


**Figure 11.**
Influence of tube diameter on the Nusselt number under different Reynolds numbers

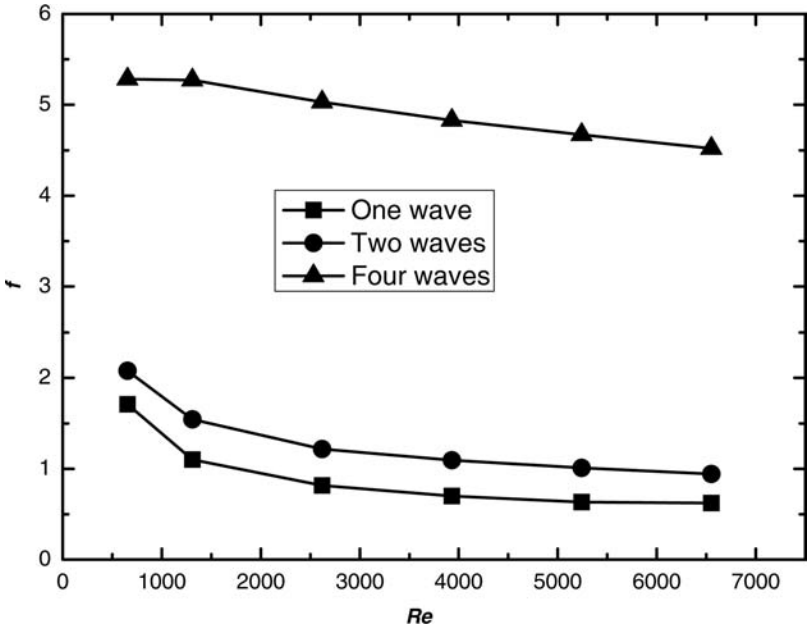


**Figure 12**
Influence of wave number on the friction factor under different Reynolds numbers

heat exchangers, especially at high Reynolds numbers. For example, at $Re \geq 3,930$ the wavy fin-and-tube heat exchanger with four waves own twice Nusselt number of that of wavy fin-and-tube heat exchanger with only one wave, while the wavy fin-and-tube

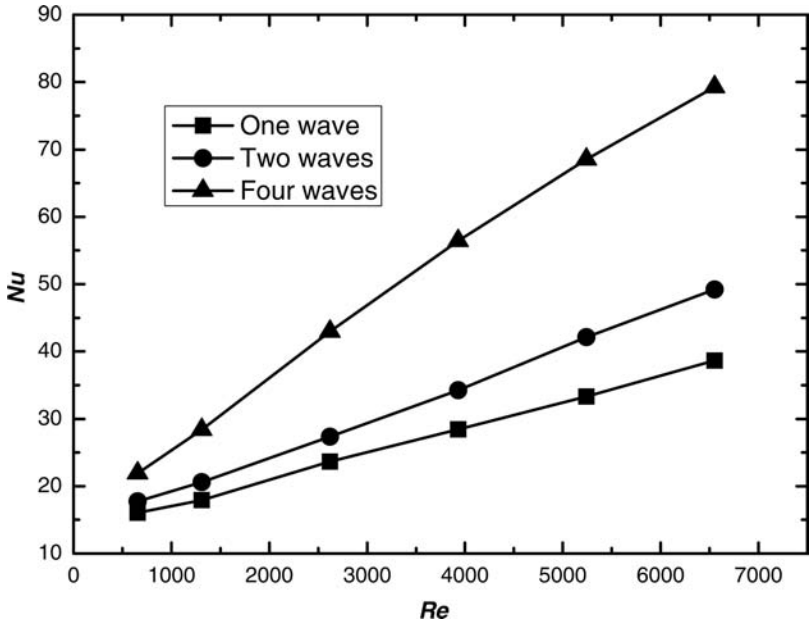


**Figure 13.**
Influence of wave density on the Nusselt number under different Reynolds numbers

heat exchanger with two waves only owns about 20 percent higher than that of wavy fin-and-tube heat exchanger with one wave.

## 4. Conclusions

In this paper, a novel CLEARER algorithm is adopted to simulate the periodically developed laminar flow in the wavy fin-and-tube heat exchanger, and the influence of wave amplitude, fin pitch, tube diameter and wave density on fluid flow and heat transfer characteristics is examined. The major findings are listed as follows:

- CLEARER algorithm is reliable and efficient in solving the complex fluid flow in the wavy fin-and-tube heat exchanger.
- Both the friction factor and Nusselt number of the wavy fin-and-tube heat exchanger increase with the increase of wave amplitude, tube diameter or wave density, while the increase rate of friction factor is higher than that of Nusselt number.
- The friction factor of the wavy fin-and-tube heat exchanger increases with the decrease of fin pitch, while the Nusselt number does not vary in the similar way. At low Reynolds number, the Nusselt number of the wavy fin-and-tube heat exchanger increases with the decrease of fin pitch, but at high Reynolds number, Nusselt number increases with the increase of fin pitch.
- Wavy fin is an effective way to enhance heat transfer in plate fin-and-tube heat exchanger.

## References

Beecher, D.T. and Fagan, T.J. (1987), "Effects of fin pattern on the air-side heat transfer coefficient in plate finned-tube heat exchangers", *ASHRAE Transaction*, Vol. 93, pp. 1961-84.

Cheng, Y.P., Lee, T.S., Low, H.T. and Tao, W.Q. (2007), "An efficient and robust numerical scheme for SIMPLER algorithm on non-orthogonal curvilinear coordinates, CLEARER", *Numerical Heat Transfer B*, Vol. 51, pp. 433-61.

Dong, J.Q., Chen, J.P., Chen, Z.J., Zhou, Y.M. and Zhang, W.F. (2007), "Heat transfer and pressure drop correlations for the wavy fin and flat tube heat exchangers", *Applied Thermal Engineering*, Vol. 27, pp. 2066-73.

Jang, J.Y. and Chen, L.K. (1997), "Numerical analysis of heat transfer and fluid flow in a three-dimensional wavy-fin and tube heat exchanger", *International Journal of Heat and Mass Transfer*, Vol. 40, pp. 3981-90.

Kang, H.C. and Webb, R.L. (1998), "Evaluation of the wavy fin geometry used in air-cooled finned tube heat exchangers", *Proceedings of the 11th International Heat Transfer Conference*, *Kyongju*, pp. 95-100.

Kang, H.J., Li, W., Li, H.J., Xin, R.C. and Tao, W.Q. (1994), "Experimental study on heat transfer and pressure drop characteristics of four types of plate fin-and-tube heat exchanger surfaces", *International Journal of Thermal and Fluid Science*, Vol. 3, pp. 34-42.

Kuvannarat, T., Wang, C.C. and Wongwises, S. (2006), "Effect of fin thickness on the air-side performance of wavy fin-and-tube heat exchangers under dehumidifying conditions", *International Journal of Heat and Mass Transfer*, Vol. 49, pp. 2587-96.

Li, Z.Y. and Tao, W.Q. (2002), "A new stability-guaranteed second-order difference scheme", *Numerical Heat Transfer B*, Vol. 42, pp. 349-65.

Min, J.C. and Webb, R.L. (2001), "Numerical predictions of wavy fin coil performance", *Journal of Enhanced Heat Transfer*, Vol. 8, pp. 159-73.

Patankar, S.V. (1980), *Numerical Heat Transfer and Fluid Flow*, McGraw-Hill, New York, NY.

Pirompugd, W., Wongwises, S. and Wang, C.C. (2006), "Simultaneous heat and mass transfer characteristics for wavy fin-and-tube heat exchangers under dehumidifying conditions", *International Journal of Heat and Mass Transfer*, Vol. 49, pp. 132-43.

Tao, W.Q. (2000), *Recent Advances in Computational Heat Transfer*, Science Press, Beijing.

Tao, W.Q. (2001), *Numerical Heat Transfer*, 2nd ed., Xi'an Jiaotong University Press, Xi'an.

Tao, Y.B., He, Y.L., Huang, J., Wu, Z.G. and Tao, W.Q. (2007a), "Numerical study of local heat transfer coefficient and fin efficiency of wavy fin-and-tube heat exchangers", *International Journal of Thermal Sciences*, Vol. 46, pp. 768-78.

Tao, Y.B., He, Y.L., Huang, J., Wu, Z.G. and Tao, W.Q. (2007b), "Three-dimensional numerical study of wavy fin-and-tube heat exchangers and field synergy principle analysis", *International Journal of Heat and Mass Transfer*, Vol. 50, pp. 1163-75.

Tao, W.Q., Cheng, Y.P. and Lee, T.S. (2007c), "3D numerical simulation on fluid flow and heat transfer characteristics in multistage heat exchanger with slit fins", *Heat and Mass Transfer*, Vol. 44, pp. 125-36.

Thomas, P.D. and Middlecoeff, J.F. (1980), "Direct control of the grid point distribution in meshes generated by elliptic equations", *AIAA Journal*, Vol. 18, pp. 652-6.

Wang, C.C., Chang, J.Y. and Chiou, N.F. (1999a), "Effects of waffle height on the air-side performance of wavy fin-and-tube heat exchangers", *Heat Transfer Engineering*, Vol. 20, pp. 45-56.

Wang, C.C., Fu, W.F. and Chang, C.T. (1997), "Heat transfer and friction characteristics of typical wavy fin-and-tube heat exchangers", *Experimental Thermal and Fluid Science*, Vol. 14, pp. 174-86.

Wang, C.C., Hwang, Y.M. and Lin, Y.T. (2002), "Empirical correlations for heat transfer and flow friction characteristics of herringbone wavy fin-and-tube heat exchangers", *International Journal of Refrigeration*, Vol. 25, pp. 673-80.

Wang, C.C., Jiang, J.Y. and Chiou, N.F. (1999b), "A heat transfer and friction correlation for wavy fin-and-tube heat exchangers", *International Journal of Heat and Mass Transfer*, Vol. 42, pp. 1919-24.

Webb, R.L. (1990), "Air-side heat transfer correlations for flat and wavy plate fin-and-tube geometries", *ASHRAE Transaction*, Vol. 96, pp. 445-9.

Wongwises, S. and Chokeman, Y. (2005), "Effect of fin pitch and number of tube rows on the air side performance of herringbone wavy fin and tube heat exchangers", *Energy Conversion and Management*, Vol. 46, pp. 2216-31.

**Corresponding author**
Y.P. Cheng can be contacted at: mpecyp@nus.edu.sg